

## Research



Article submitted to journal

**Subject Areas:**  
fluid mechanics

**Keywords:**  
separated flows, flow control,  
adjoint-based control

**Author for correspondence:**  
E. Boujo  
e-mail: [edouard.boujo@epfl.ch](mailto:edouard.boujo@epfl.ch)

# Manipulating flow separation: sensitivity of stagnation points, separatrix angles and recirculation area to steady actuation

E. Boujo and F. Gallaire

Laboratory of Fluid Mechanics and Instabilities  
École Polytechnique Fédérale de Lausanne  
CH-1015 Lausanne, Switzerland

A variational technique is used to derive analytical expressions for the sensitivity of several geometric indicators of flow separation to steady actuation. Considering the boundary layer flow above a wall-mounted bump, the six following representative quantities are considered: the locations of the separation point and reattachment point connected by the separatrix, the separation angles at these stagnation points, the backflow area and the recirculation area. For each geometric quantity, linear sensitivity analysis allows us to identify regions which are the most sensitive to volume forcing and wall blowing/suction. Validations against full non-linear Navier–Stokes calculations show excellent agreement for small-amplitude control for all considered indicators. With very resemblant sensitivity maps, the reattachment point, the backflow and recirculation areas are seen to be easily manipulated. In contrast, the upstream separation point and the separatrix angles are seen to remain extremely robust with respect to external steady actuation.

## 1. Introduction

Flow separation leads in many aerodynamic situations to performance loss, such as reduced lift, increased drag, enhanced fluctuations or noise production. In contrast, separation yields a recirculation region that is often desirable in combustion devices. It is thus not a surprise that there is extensive research on the control of flow separation [1]. Attempts include, in decreasing order of complexity, closed-loop separation control, harmonic or steady active open-loop control and passive control devices.

Studies on closed loop control strategies remain few: while Alam, Liu & Haller [2] have provided an analytical approach to closed-loop separation control, based on a kinematic theory of unsteady separation [3], most experimental approaches rely either on low-order reduced models, extracted by physical means or using identification methods [4], or the design of black box controllers [5,6].

Open-loop control has been successfully applied to separation control: harmonically pulsed synthetic jets [7,8], as well as steady suction or blowing at the wall (e.g. [9] and other references in [10], or [11] as a combination of steady suction and pulsed blowing). The determination of the best placement and frequency of the actuators was often left to extensive parameter sweeps resorting to intensive experimental or computational campaigns.

Passive control strategies rely on the optimisation of the geometry or on the addition of appendices, like vortex generators [12]. Their efficient and robust design requires ideally so-called sensitivity maps. These maps allow one to choose most sensitive regions and therefore to design optimal control configurations, but again to the expense of intensive experimental or computational campaigns. A recent example is provided by Parezanović & Cadot [13], who studied the influence of a thin control wire on the frequency, drag and recirculation length of the wake behind a D-shaped cylinder.

In all these control methods, an essential aspect is determining meaningful and unambiguous control variables. Among those the manipulation of the separation or reattachment locations [2, 14], the recirculation length [15] or the recirculation area [6] appear as valuable and accessible geometric descriptors of the flow. The existence of a link between the geometric properties of separated flows and their stability properties and associated aerodynamic loads is indeed now well accepted.

It is known for instance that the destabilisation of the wake of a bluff body beyond the critical Reynolds number takes place simultaneously with a decrease of the recirculation length caused by the mean flow distortion maintained by the progressive development of the instability [16]. Therefore, if one is willing to enhance mixing or reduce flow-induced structural vibrations, then it is natural to target the recirculation length. More recently, Parezanović & Cadot [13] established a clear correlation between base pressure increase (and therefore drag reduction) and mean recirculation area increase in the wake of a D-shaped cylinder at  $Re \sim 10^5$ , suggesting the direct targeting of the separation properties as a promising control strategy. It is also worth noticing that, in some control attempts [17,18], without being directly targeted, a modification of the recirculation length was observed as a by-product of the control scheme.

The present study is dedicated to the determination of analytical expressions for the sensitivity to steady actuation of the following six geometric indicators of flow separation: the locations of the two separation points which connect the separatrix, the separation angles prevailing at these separation points, the backflow area and the recirculation area. These geometric quantities can easily be measured in experiments. Sensitivity maps are computed by solving adjoint equations at the same cost as that of computing the uncontrolled flow, and these maps allow one to identify sensitive regions and predict the effect of small-amplitude control without actually computing any controlled flow. The main focus of this study is on the rigorous derivation of sensitivity expressions for steady control, which constitutes a first step towards more general unsteady control. The flow configuration considered is the boundary layer flow above a wall-mounted

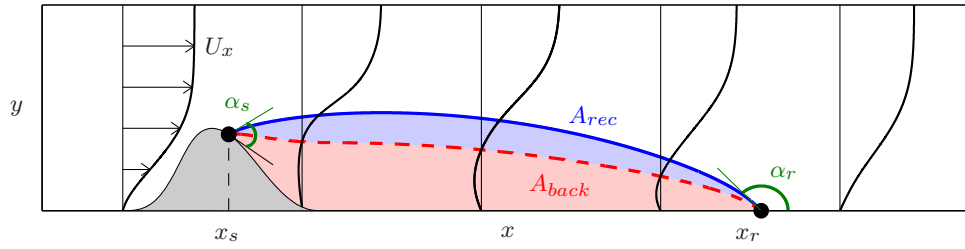


**Figure 1.** Sketch of the bump flow. The flow separates at  $x_s$  and reattaches at  $x_r$  (black dots). The separatrix (blue solid line) encloses the recirculation region (blue shade) of area  $A_{rec}$  and makes angles  $\alpha_s$ ,  $\alpha_r$  with the wall. Velocity profiles are shown with black lines. The curve where  $U_x = 0$  (red dashed line) delimits the backflow area (red shade) of area  $A_{back}$ . The bump wall geometry is parametrised by  $y_w(x)$  and the separatrix by  $y_{sep}(x)$ . The axes are not to scale.

bump, on which several open-loop [19] and closed-loop [18] control strategies have been tested numerically.

This paper is organised as follows: geometric quantities of interest are introduced in section 2; the concept of sensitivity analysis is presented in section 3; expressions of sensitivity to base flow modification are derived in section 4; results and validation for volume control and wall control are given in section 5.

## 2. Characteristic quantities in separated flows

The evolution of the recirculation length in separated flows with the increase in Reynolds number  $Re$  is well documented [16,20–26]. For instance, in the flow around a circular cylinder, the recirculation length is known to increase with  $Re$  in the steady laminar regime while it starts to decrease in mean value as  $Re$  is further increased in the unsteady laminar regime. In the present study, we turn our attention to several characteristic quantities which describe the separation, in complement to the recirculation length: the locations of the two separation points ( $x_s$  and  $x_r$ ) which connect the separatrix, the separation angles ( $\alpha_s$  and  $\alpha_r$ ) prevailing at these separation points, the backflow area  $A_{back}$  and the recirculation area  $A_{rec}$ .

As an archetypical flow configuration, we consider the boundary layer flow above a wall-mounted bump studied through DNS [24] and through global stability analysis [27].

Figure 1 is a schematic of typical flow separation. The recirculation region is delimited by the wall and the separating streamline. This particular streamline, or *separatrix*, makes angles  $\alpha_s$  and  $\alpha_r$  at the separation point  $x_s$  and reattachment point  $x_r$ , respectively. The wall geometry is described by  $y_w(x)$  and the separatrix by  $y_{sep}(x)$ . Unit vectors tangent and normal to the wall are noted  $\mathbf{t}$  and  $\mathbf{n}$  (figure 2), and  $\partial_t$ ,  $\partial_n$  stand for derivatives along  $\mathbf{t}$  and  $\mathbf{n}$ .

In this paper we focus on the following quantities:

- (i) The location of stagnation points, i.e. separation point  $x_s$  and reattachment point  $x_r$ , characterised by zero wall shear stress

$$\tau_{s/r} = \partial_n U_t(\mathbf{x}_{s/r}) = 0; \quad (2.1)$$

- (ii) The angle between the separatrix and the wall at the separation and reattachment points, given by Lighthill's formula [28]

$$\tan(\alpha_{s/r}) = -3 \frac{\partial_{nt} U_t}{\partial_{nn} U_t} \Big|_{\mathbf{x}_{s/r}}; \quad (2.2)$$

- (iii) The area of the backflow region

$$A_{back} = \iint_{\Omega} \mathbb{1}_{\Omega_{back}}(\mathbf{x}) \, d\Omega \quad (2.3)$$

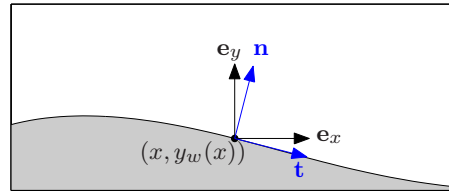


**Figure 2.** Sketch of tangent and normal vectors to the wall at  $(x, y) = (x, y_w(x))$ .

where  $\mathbb{1}_{\Omega_{back}}$  is the characteristic function of  $\Omega_{back} = \{(x, y) \mid U_x < 0\}$ ;

(iv) The area of the recirculation region enclosed between the separatrix and the wall

$$A_{rec} = \iint_{\Omega} \mathbb{1}_{\Omega_{rec}}(\mathbf{x}) \, d\Omega \quad (2.4)$$

where  $\mathbb{1}_{\Omega_{rec}}$  is the characteristic function of  $\Omega_{rec} = \{(x, y) \mid x_s \leq x \leq x_r, y_w(x) \leq y \leq y_{sep}(x)\}$ .

The steady-state flow  $\mathbf{U}(\mathbf{x})$  is calculated by solving the Navier–Stokes equations with a finite element method and an iterative Newton procedure on a mesh highly refined near stagnation points. A two-dimensional triangulation of the computational domain is generated with the finite element software *FreeFem++* (<http://www.freefem.org>), and equations are solved in their variational formulation, with the following boundary conditions: Blasius profile at the inlet, no-slip condition on the wall, symmetry condition at the top border, and convective condition  $-P\mathbf{n} + Re^{-1}\nabla\mathbf{U}\mathbf{n} = \mathbf{0}$  at the outlet. P2 and P1 Taylor-Hood elements are used for spatial discretisation of velocity and pressure, respectively (see also details and validation in [19] and [15]). Stagnation points are found according to (2.1) with a bisection on the wall shear stress  $\partial_n U_t$ . Angles are calculated using Lighthill's formula (2.2), and are found to agree very well with geometric angles measured between the wall and the separatrix integrated from  $\mathbf{U}(\mathbf{x})$  with a fourth-order Runge-Kutta method. Areas (2.3)–(2.4) are computed with a trapezoidal rule for the two-dimensional integration of the backflow region and recirculation region.

Figure 3 illustrates how the backflow and recirculation regions grow with Reynolds number in the bump flow. Figure 4 shows that the reattachment point moves downstream linearly with  $Re$ , which is typical of steady separated flows. The areas  $A_{back}$  and  $A_{rec}$  show the same trend but increase more than linearly since the backflow and recirculation regions become not only much longer but also slightly higher. The separation point moves a little upstream but stays downstream of the bump summit ( $x_b = 25$ ). The reattachment angle is fairly constant,  $180 - \alpha_r \simeq 13 - 15^\circ$ . The separation angle measured relative to the wall decreases from  $\alpha_s = 19^\circ$  to  $13^\circ$  between  $Re = 100$  and 700, but measured relative to  $\mathbf{e}_x$  it is small and almost constant,  $\alpha_s + \theta_{wall} \simeq 6 - 8^\circ$ . It is interesting to note that the separatrix angles vary slowly with  $Re$  even though the recirculation length increases significantly. These observations indicate that the main effect of  $Re$  is to elongate the recirculation region, while the flow remains mostly horizontal.

### 3. Sensitivity analysis

In this section, analytical expressions are given for the sensitivity of quantities of interest (2.1)–(2.4) to flow modifications, volume forcing and blowing/suction at the wall.

The sensitivity to flow modification of a quantity of interest, say  $\phi$ , is a field defined through the first-order variation  $\delta\phi$  induced by a small flow modification  $\delta\mathbf{U}$ ,

$$\delta\phi = (\nabla_{\mathbf{U}}\phi \mid \delta\mathbf{U}), \quad (3.1)$$

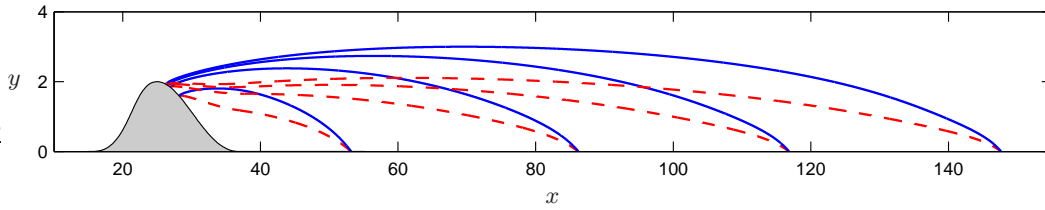


**Figure 3.** Separatrix (blue solid line) and curve of zero streamwise velocity  $U_x = 0$  (red dashed line), at  $Re = 100, 300, 500$  and  $700$ . The axes are not to scale.

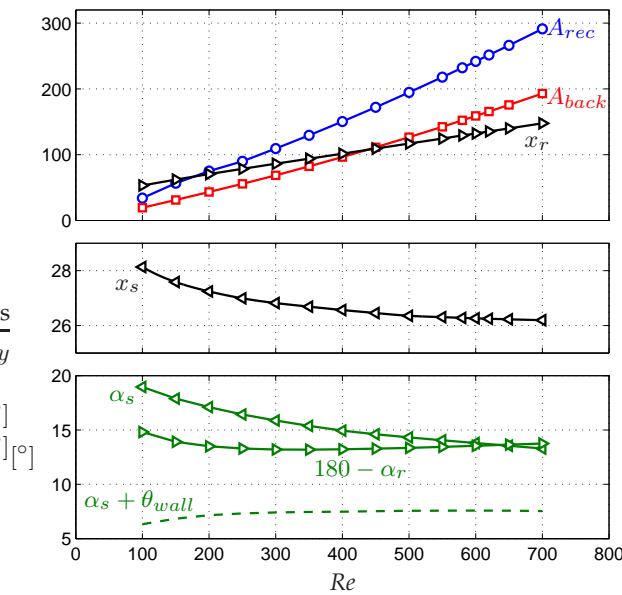


**Figure 4.** Variation with Reynolds number of characteristic separation quantities: recirculation and backflow areas  $A_{rec}$  and  $A_{back}$ , separation and reattachment locations  $x_s$  and  $x_r$ , separation and reattachment angles  $\alpha_s$  and  $\alpha_r$  relative to the wall (the dashed line shows the “absolute” separation angle  $\alpha_s + \theta_{wall}$ , i.e. measured relative to  $e_x$ ).

and it can be computed as:

$$\frac{d\phi}{d\mathbf{U}} \delta\mathbf{U} = \lim_{\epsilon \rightarrow 0} \frac{\phi(\mathbf{U} + \epsilon \delta\mathbf{U}) - \phi(\mathbf{U})}{\epsilon}. \quad (3.2)$$

Here  $(\mathbf{a} | \mathbf{b}) = \iint_{\Omega} \mathbf{a} \cdot \mathbf{b} \, d\Omega$  denotes the two-dimensional inner product in  $\Omega$ . In other words, the sensitivity  $\nabla_{\mathbf{U}} \phi = d\phi/d\mathbf{U}$  is the gradient of  $\phi$  with respect to flow modification. Analytical expressions for the sensitivity to flow modification of the geometric quantities of interest considered in this study will be derived in section 4 (see (4.10) for the location of stagnation points, (4.24) for separatrix angles, and (4.36)-(4.42) for backflow area and recirculation area).

In practice, the base flow cannot be modified arbitrarily and one has to resort to an external control, e.g. passive obstacle, heating, magnetic field, geometry modification, wall motion, wall blowing or suction, etc. This control in turn alters the velocity field. Here we focus on steady control, either in the domain  $\Omega$  by means of a body force (source of momentum)  $\mathbf{C}$ , or at the wall  $\Gamma_w$  by means of blowing/suction with velocity  $\mathbf{U}_c$ . However the method is general and easily handles other types of control.

Sensitivities to volume control and wall control can be defined through the variation  $\delta\phi$  induced by small-amplitude control,

$$\delta\phi = (\nabla_{\mathbf{C}}\phi | \delta\mathbf{C}) + \langle \nabla_{\mathbf{U}_c}\phi | \delta\mathbf{U}_c \rangle, \quad (3.3)$$

where  $\langle \mathbf{a} | \mathbf{b} \rangle = \int_{\Gamma_w} \mathbf{a} \cdot \mathbf{b} \, d\Gamma$  denotes the one-dimensional inner product on  $\Gamma_w$ . Sensitivities  $\nabla_{\mathbf{C}}\phi = d\phi/d\mathbf{C}$  and  $\nabla_{\mathbf{U}_c}\phi = d\phi/d\mathbf{U}_c$  can be computed as:

$$\frac{d\phi}{d\mathbf{C}}\delta\mathbf{C} = \lim_{\epsilon \rightarrow 0} \frac{\phi(\mathbf{C} + \epsilon\delta\mathbf{C}) - \phi(\mathbf{C})}{\epsilon}, \quad \frac{d\phi}{d\mathbf{U}_c}\delta\mathbf{U}_c = \lim_{\epsilon \rightarrow 0} \frac{\phi(\mathbf{U}_c + \epsilon\delta\mathbf{U}_c) - \phi(\mathbf{U}_c)}{\epsilon}. \quad (3.4)$$

Taking into account the definition of  $\phi$ , and enforcing the Navier–Stokes equations to be satisfied by the flow, a Lagrangian method yields the sensitivities

$$\nabla_{\mathbf{C}}\phi = \mathbf{U}^\dagger, \quad \nabla_{\mathbf{U}_c}\phi = -P^\dagger \mathbf{n} - Re^{-1} \nabla \mathbf{U}^\dagger \mathbf{n}, \quad (3.5)$$

where the adjoint flow  $(\mathbf{U}^\dagger, P^\dagger)^T$  is solution of the non-homogeneous linear equations

$$\nabla \cdot \mathbf{U}^\dagger = 0, \quad -\mathbf{U} \cdot \nabla \mathbf{U}^\dagger + \mathbf{U}^\dagger \cdot \nabla \mathbf{U}^T - \nabla P^\dagger - Re^{-1} \nabla^2 \mathbf{U}^\dagger = \nabla_{\mathbf{U}}\phi, \quad (3.6)$$

with boundary condition  $\mathbf{U}^\dagger = \mathbf{0}$  at the wall. The forcing term in (3.6) is the sensitivity of  $\phi$  to flow modification defined in (3.1)–(3.2), which must therefore be computed beforehand, using expressions derived in detail in section 4 for all quantities of interest (2.1)–(2.4). Using the same finite element method as for the determination of the base flow, sensitivities (3.5) are obtained by solving the adjoint equations (3.6) in weak form, particularly convenient to express the forcing term  $\nabla_{\mathbf{U}}\phi$ .

## 4. Derivation of sensitivities to flow modification

In this section, analytical expressions are derived for the sensitivity of quantities of interest (2.1)–(2.4) to flow modification. Recall that the wall  $\Gamma_w$  is parametrised by  $(x, y) = (x, y_w(x))$ , as shown in figure 2.

### (a) Stagnation points

As expressed in (2.1), steady separation and reattachment points  $\mathbf{x}_s = (x_s, y_w(x_s))$  and  $\mathbf{x}_r = (x_r, y_w(x_r))$  are characterised by zero wall shear stress. Following [15], stagnation points are redefined in terms of characteristic functions:

$$x_s = \int_0^{x^*} H(\tau(x)) \, dx = \int_0^{x^*} G(x) \, dx, \quad (4.1)$$

$$x_r = \int_{x^*}^{\infty} H(-\tau(x)) \, dx + x^* = \int_{x^*}^{\infty} 1 - G(x) \, dx + x^*, \quad (4.2)$$

where  $\tau(x) = \partial_n U_t|_{(x, y_w(x))}$  is the wall shear stress,  $H$  is the Heaviside step function defined as  $H(\gamma < 0) = 0$ ,  $H(\gamma > 0) = 1$ , and  $x^*$  is any streamwise location inside the recirculation region. As illustrated in figure 5, the integrand in (4.1) is equal to 1 upstream of the separation point, therefore integrating over  $0 \leq x \leq x^*$  does indeed yield the coordinate  $x_s$ . Similarly, the integrand in (4.2) is equal to 1 upstream of the reattachment point, and integrating in  $x$  yields the coordinate  $x_r$ .

We assume for the sake of clarity that reattachment occurs far enough downstream where the wall is horizontal and  $\tau(x_r) = \partial_y U_x|_{(x_r, y_w(x_r))}$ , which is verified in practice for all the Reynolds numbers considered. A flow modification  $\delta\mathbf{U}$  makes the reattachment point move by

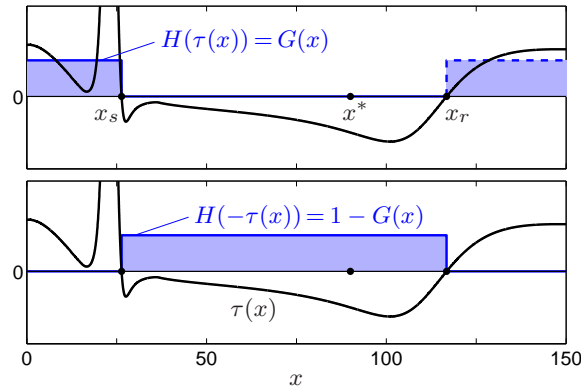


**Figure 5.** Wall shear stress and associated Heaviside functions appearing in the expression of the stagnation points (4.1)-(4.2).

the following amount:

$$\delta x_r = \lim_{\epsilon \rightarrow 0} \frac{x_r(\mathbf{U} + \epsilon \delta \mathbf{U}) - x_r(\mathbf{U})}{\epsilon} \quad (4.3)$$

$$= \lim_{\epsilon \rightarrow 0} \frac{1}{\epsilon} \int [H(-\tau(x) - \epsilon \delta \tau(x)) - H(-\tau(x))] dx \quad (4.4)$$

$$= \int - \left. \frac{dH}{d\gamma} \right|_{\gamma=-\tau(x)} \delta \tau(x) dx \quad (4.5)$$

$$= \int - \left( \frac{d\tau}{dx}(x) \right)^{-1} \frac{dG}{dx}(x) \delta \tau(x) dx \quad (4.6)$$

$$= \int - \left( \frac{d\tau}{dx}(x) \right)^{-1} \delta(x - x_r) \delta \tau(x) dx \quad (4.7)$$

$$= - \frac{\delta \tau(x_r)}{d_x \tau|_{(x_r, y_w(x_r))}} \quad (4.8)$$

where (4.6) comes from the chain rule differentiation  $\frac{d(1-G)}{dx}(x) = - \left. \frac{dH}{d\gamma} \right|_{\gamma=-\tau(x)} \frac{d\tau}{dx}(x)$ , and (4.7) is the result of  $\frac{dG}{dx}(x) = \delta(x - x_r)$  with  $\delta(x)$  the Dirac delta function, since  $G$  increases from 0 to 1 at  $x = x_r$ . Finally:

$$\delta x_r = (\nabla_{\mathbf{U}} x_r | \delta \mathbf{U}) = - \left. \frac{\partial_y \delta U_x}{\partial_{xy} U_x} \right|_{\mathbf{x}_r}. \quad (4.9)$$

The variation of the separation point is obtained in a similar way, with only slight sign differences. First, the chain rule derivation of  $G(x) = H(\tau(x))$  reads  $\frac{dG}{dx}(x) = \left. \frac{dH}{d\gamma} \right|_{\gamma=\tau(x)} \frac{d\tau}{dx}(x)$ .

Second, the expression in terms of Dirac delta is  $\frac{dG}{dx}(x) = -\delta(x - x_s)$  since  $G$  decreases from 1 to 0 at  $x = x_s$ . Taking into account the wall geometry, one obtains:

$$\delta x_s = (\nabla_{\mathbf{U}} x_s | \delta \mathbf{U}) = - \left. \frac{1}{\sqrt{1 + y_w'^2}} \frac{\partial_n \delta U_t}{\partial_{nt} U_t} \right|_{\mathbf{x}_s} \quad (4.10)$$

where  $y_w' = dy_w/dx$ . Expression (4.10) is valid for the reattachment point too, where  $y_w' = 0$ ,  $\mathbf{t} \equiv \mathbf{e}_x$ , and  $\mathbf{n} \equiv \mathbf{e}_y$ .

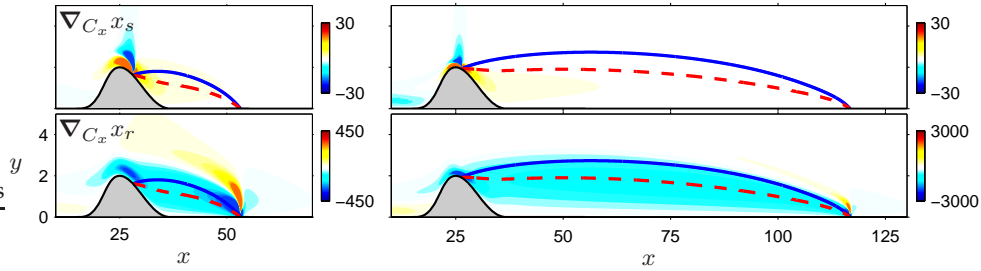


**Figure 6.** Sensitivity of stagnation points  $x_s$ ,  $x_r$ , with respect to streamwise volume control  $C_x$ . Left:  $Re = 100$ , right:  $Re = 500$ . The blue solid line is the separatrix, the red dashed line is the curve where  $U_x = 0$ .

Figure 6 shows the sensitivity of stagnation points to volume control in the streamwise direction  $C_x = \mathbf{C} \cdot \mathbf{e}_x$  obtained at  $Re = 100$  and  $500$  using (4.9)-(4.10) and the method presented in section 3. Red (resp. blue) regions indicate where a localised, small-amplitude body force oriented along  $\mathbf{e}_x$  would move stagnation points upstream,  $\delta x_{s/r} > 0$  (resp. downstream,  $\delta x_{s/r} < 0$ ). The separation point is mostly sensitive near  $\mathbf{x}_s$ . The reattachment point is sensitive near  $\mathbf{x}_r$ , but also at the bump summit, in the whole shear layer along the separatrix, and in the recirculation region.

## (b) Separation and reattachment angles

It is remarkable but not well known that the angle between the separatrix and the wall can be expressed analytically as a function of flow quantities at the stagnation point, as expressed in (2.2). We recall briefly Lighthill's original presentation [28]. For the sake of simplicity we assume first that the wall is flat and horizontal,  $y_w(x) = 0$ . A Taylor expansion of the streamwise velocity near the wall,  $y \ll 1$ , reads

$$U_x(x, y) = U_x(x, 0) + \partial_y U_x(x, 0) y + \frac{\partial_{yy} U_x(x, 0)}{2} y^2 + \mathcal{O}(y^3). \quad (4.11)$$

This expression is conveniently recast using (i) the no-slip condition  $U_x(x, 0) = 0$ , (ii) the vorticity  $\omega(x, 0) = -\partial_y U_x(x, 0)$ , and (iii) the streamwise momentum equation  $\partial_{yy} U_x(x, 0) = Re \partial_x p(x, 0)$ :

$$U_x(x, y) = -\omega(x, 0) y + \frac{Re}{2} \partial_x p(x, 0) y^2 + \mathcal{O}(y^3). \quad (4.12)$$

Equivalently, the stream function defined as  $U_x = \partial_y \psi$  reads

$$\psi(x, y) = -\frac{1}{2} \omega(x, 0) y^2 + \frac{Re}{6} \partial_x p(x, 0) y^3 + \mathcal{O}(y^4). \quad (4.13)$$

The separatrix  $\psi = 0$  is thus described by  $y_{sep}(x) = 3\omega(x, 0)/Re \partial_x p(x, 0)$  and separates from or reattaches to the wall with the angle  $\alpha$  such that

$$\begin{aligned} \tan(\alpha) &= \frac{dy_{sep}}{dx} = \frac{3}{Re} \left( \frac{\partial_x \omega}{\partial_x p} - \omega \frac{\partial_{xx} p}{(\partial_x p)^2} \right) \\ &= \frac{3}{Re} \frac{\partial_x \omega}{\partial_x p} = -3 \frac{\partial_{xy} U_x}{\partial_{yy} U_x} \end{aligned} \quad (4.14)$$

because  $\omega(x_{s/r}, 0) = 0$ . Equation (4.14) is valid for a curved or inclined wall too, hence recovering (2.2). A longer but similar derivation is possible following the steps of [3] for unsteady flows, and of course the same expression is also obtained if taking all quantities as steady in his final expression.

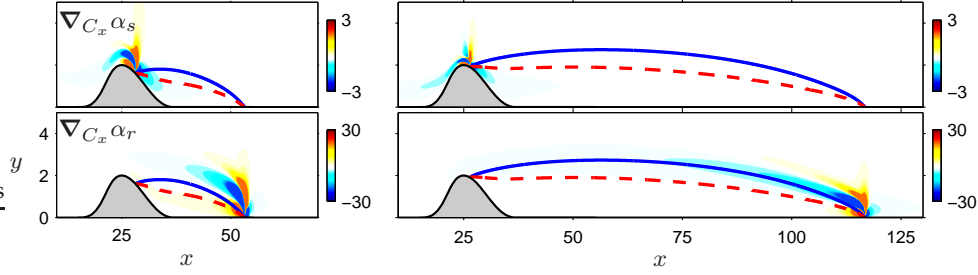


**Figure 7.** Sensitivity of separation and reattachment angles  $\alpha_s, \alpha_r$ , with respect to streamwise volume control  $C_x$ . Left:  $Re = 100$ , right:  $Re = 500$ . The blue solid line is the separatrix, the red dashed line is the curve where  $U_x = 0$ .

To derive the sensitivity of the angle, we introduce the function  $f$  defined on the wall

$$f(\mathbf{U}, x) = \tan^{-1} \left( -3 \frac{\partial_{nt} U_t}{\partial_{nn} U_t} \Big|_{(x, y_w(x))} \right), \quad (4.15)$$

where  $\mathbf{U}$  and  $x$  are treated as independent variables. The separation and reattachment angles are equal to  $\alpha_{s/r} = f(\mathbf{U}, x_{s/r})$ . Their variation with flow modification is

$$\delta \alpha_{s/r} = (\nabla_{\mathbf{U}} \alpha_{s/r} | \delta \mathbf{U}) = \left( \frac{\partial f}{\partial \mathbf{U}} + \frac{\partial f}{\partial x} \Big|_{x_{s/r}} \frac{dx_{s/r}}{d\mathbf{U}} \Big| \delta \mathbf{U} \right), \quad (4.16)$$

where the first term of the sensitivity is the direct angle variation due to the change in tangential velocity  $U_t$ , while the second term is the indirect angle variation due to the displacement of the stagnation points  $x_{s/r}$ . Before deriving in detail each of the terms of (4.16) we give their expression below:

$$\left( \frac{\partial f}{\partial \mathbf{U}} \Big| \delta \mathbf{U} \right) = -3 \frac{A \partial_{nt} \delta U_t - B \partial_{nn} \delta U_t}{A^2 + 9B^2} \Big|_{\mathbf{x}_{s/r}}, \quad (4.17)$$

$$\frac{\partial f}{\partial x} \Big|_{\mathbf{x}_{s/r}} \delta x_{s/r} = -3 \frac{B'A - A'B}{A^2 + 9B^2} \delta x_{s/r}, \quad (4.18)$$

$$\delta x_{s/r} = \left( \frac{dx_{s/r}}{d\mathbf{U}} \Big| \delta \mathbf{U} \right) = (\nabla_{\mathbf{U}} x_{s/r} | \delta \mathbf{U}), \quad (4.19)$$

where

$$A(x) = \partial_{nn} U_t(x, y_w(x)), \quad (4.20)$$

$$B(x) = \partial_{nt} U_t(x, y_w(x)), \quad (4.21)$$

$$A'(x) = 3 \frac{y_w''}{1 + y_w'^2} \partial_{nn} U_n + \sqrt{1 + y_w'^2} \partial_{nn} U_t, \quad (4.22)$$

$$B'(x) = \frac{y_w''}{1 + y_w'^2} (\partial_{nn} U_t + 2\partial_{nt} U_n) - \sqrt{1 + y_w'^2} \partial_{nn} U_n. \quad (4.23)$$

Combining equations (4.16)-(4.23) yields:

$$\begin{aligned} \delta \alpha_{s/r} &= (\nabla_{\mathbf{U}} \alpha_{s/r} | \delta \mathbf{U}) \\ &= -\frac{3}{A^2 + 9B^2} \left( A \partial_{nt} - B \partial_{nn} + \frac{A'B - B'A}{B \sqrt{1 + y_w'^2}} \partial_n \right) \delta U_t \Big|_{\mathbf{x}_{s/r}}. \end{aligned} \quad (4.24)$$

Figure 7 shows the sensitivity of separatrix angles to streamwise volume control obtained at  $Re = 100$  and  $500$  using (4.24). Like stagnation points, the separation angle is mostly sensitive

near  $\mathbf{x}_s$ , and the reattachment angle near  $\mathbf{x}_r$ . These sensitivity maps show complex structures, with regions of opposite signs close to each other. This indicates that a small displacement of the forcing location could result in changing the sign of the variation  $\delta\alpha$ .

We now turn to the derivation of the three terms in (4.16). The latter term (4.19) is precisely the variation of stagnation points (4.9)-(4.10). Next, the variation of  $f$  with flow modification (at fixed  $x$ ) is:

$$\delta f = \left( \frac{\partial f}{\partial \mathbf{U}} \middle| \delta \mathbf{U} \right) = \lim_{\epsilon \rightarrow 0} \frac{f(\mathbf{U} + \epsilon \delta \mathbf{U}, x_{s/r}) - f(\mathbf{U}, x_{s/r})}{\epsilon}, \quad (4.25)$$

where, at first order:

$$\begin{aligned} f(\mathbf{U} + \epsilon \delta \mathbf{U}, x_{s/r}) &= \tan^{-1} \left( -3 \frac{\partial_{nt}(U_t + \epsilon \delta U_t)}{\partial_{nn}(U_t + \epsilon \delta U_t)} \right) \\ &= \tan^{-1} \left( -3 \frac{\partial_{nt} U_t}{\partial_{nn} U_t} - 3\epsilon \frac{\partial_{nn} U_t \partial_{nt} \delta U_t - \partial_{nt} U_t \partial_{nn} \delta U_t}{(\partial_{nn} U_t)^2} \right) \\ &= \tan^{-1} \left( -3 \frac{\partial_{nt} U_t}{\partial_{nn} U_t} \right) - \frac{3\epsilon}{1 + \left( -3 \frac{\partial_{nt} U_t}{\partial_{nn} U_t} \right)^2} \frac{\partial_{nn} U_t \partial_{nt} \delta U_t - \partial_{nt} U_t \partial_{nn} \delta U_t}{(\partial_{nn} U_t)^2} \\ &= \tan^{-1} \left( -3 \frac{\partial_{nt} U_t}{\partial_{nn} U_t} \right) - 3\epsilon \frac{\partial_{nn} U_t \partial_{nt} \delta U_t - \partial_{nt} U_t \partial_{nn} \delta U_t}{(\partial_{nn} U_t)^2 + 9(\partial_{nt} U_t)^2}, \end{aligned} \quad (4.26)$$

which yields expression (4.17).

Finally, the variation of  $f(\mathbf{U}, x) = \tan^{-1}(-3B(x)/A(x))$  with  $x$  (for fixed flow conditions) is derived in a similar way, with straightforward composition of derivatives of  $\tan^{-1}$  and of a quotient:

$$\delta f = \left. \frac{\partial f}{\partial x} \right|_{x_{s/r}} \delta x_{s/r} = -3 \frac{1}{1 + (3B/A)^2} \frac{AB' - BA'}{A^2} \quad (4.27)$$

$$= -3 \frac{B'A - A'B}{A^2 + 9B^2} \delta x_{s/r}, \quad (4.28)$$

which yields expression (4.18). However, some care is needed when computing the derivatives of  $A$  and  $B$ . Although the streamwise derivative of the *total* velocity field at the wall  $\partial_x \mathbf{U}$  is related in a simple way to the tangential derivative  $\partial_t \mathbf{U}$  by geometric considerations,

$$d_x \mathbf{U}|_{(x, y_w(x))} = (\partial_x + y'_w \partial_y) \mathbf{U} = \sqrt{1 + y_w'^2} \partial_t \mathbf{U}, \quad (4.29)$$

this is true neither for *individual* velocity components nor for velocity *derivatives*. For example:

$$d_x(\partial_n U_t)|_{(x, y_w(x))} \neq (\partial_x + y'_w \partial_y)(\partial_n U_t) = \sqrt{1 + y_w'^2} \partial_t(\partial_n U_t). \quad (4.30)$$

This is because the tangential velocity  $U_t = \mathbf{U} \cdot \mathbf{t}$  depends on  $x$  not only through  $\mathbf{U}$  but also through the local tangent vector  $\mathbf{t} = \mathbf{t}(x) = \mathbf{t}(x, y_w(x))$ . Similarly, the normal derivative  $\partial_n = \nabla \cdot \mathbf{n}$  depends on  $x$  because the normal vector  $\mathbf{n} = \mathbf{n}(x) = \mathbf{n}(x, y_w(x))$  does. In (4.30), one must therefore take into account  $d_x \mathbf{t}$  and  $d_x \partial_n$ . The calculation is straightforward but tedious when expressing all quantities in the basis  $(\mathbf{e}_x, \mathbf{e}_y)$ ; instead, one can make a systematic use of the nabla

operator:

$$\begin{aligned}
d_x(\partial_n U_t) &= d_x((\nabla \cdot \mathbf{n})(\mathbf{U} \cdot \mathbf{t})) \\
&= \nabla \cdot (d_x \mathbf{n})(\mathbf{U} \cdot \mathbf{t}) + (\nabla \cdot \mathbf{n})(d_x \mathbf{U} \cdot \mathbf{t}) + (\nabla \cdot \mathbf{n})(\mathbf{U} \cdot d_x \mathbf{t}) \\
&= \nabla \cdot \left( -\frac{y_w''}{1+y_w'^2} \mathbf{t} \right) (\mathbf{U} \cdot \mathbf{t}) + (\nabla \cdot \mathbf{n}) \left( \sqrt{1+y_w'^2} \partial_t \mathbf{U} \cdot \mathbf{t} \right) + (\nabla \cdot \mathbf{n}) \left( \mathbf{U} \cdot \frac{y_w''}{1+y_w'^2} \mathbf{n} \right) \\
&= -\frac{y_w''}{1+y_w'^2} \partial_t U_t + \sqrt{1+y_w'^2} \partial_{nt} U_t + \frac{y_w''}{1+y_w'^2} \partial_n U_n \\
&= \frac{y_w''}{1+y_w'^2} (\partial_n U_n - \partial_t U_t) + \sqrt{1+y_w'^2} \partial_{nt} U_t.
\end{aligned} \tag{4.31}$$

Compared to (4.30), two additional terms coming from the derivatives of  $\partial_n$  and  $\mathbf{t}$  clearly appear. The calculation of  $A'$  and  $B'$  follows similar steps.

### (c) Backflow area

The backflow area (2.3) can be expressed as

$$A_{back} = \iint_{\Omega} \mathbb{1}_{\Omega_{back}}(\mathbf{x}) d\Omega = \iint_{\Omega} H(-U_x(\mathbf{x})) d\Omega. \tag{4.32}$$

Its sensitivity is derived in the same vein as that of stagnation points (section 4(a)):

$$\begin{aligned}
\delta A_{back} &= \lim_{\epsilon \rightarrow 0} \frac{A_{back}(\mathbf{U} + \epsilon \delta \mathbf{U}) - A_{back}(\mathbf{U})}{\epsilon} \\
&= \lim_{\epsilon \rightarrow 0} \frac{1}{\epsilon} \iint_{\Omega} [H(-U_x(\mathbf{x}) - \epsilon \delta U_x(\mathbf{x})) - H(-U_x(\mathbf{x}))] d\Omega \\
&= \iint_{\Omega} -\left. \frac{dH}{du} \right|_{u=-U_x} \delta U_x(\mathbf{x}) d\Omega \\
&= \iint_{\Omega} (\partial_n U_x)^{-1} (\nabla \mathbb{1}_{\Omega_{back}}(\mathbf{x}) \cdot \mathbf{n}) \delta U_x(\mathbf{x}) d\Omega \\
&= \iint_{\Omega} -(\partial_n U_x)^{-1} \delta_{\Gamma_{back}}(\mathbf{x}) \delta U_x(\mathbf{x}) d\Omega \\
&= -\oint_{\Gamma_{back}} \frac{\delta U_x}{\partial_n U_x} d\Gamma,
\end{aligned} \tag{4.33}$$

where  $\Gamma_{back}$  is the boundary of the backflow region  $\Omega_{back}$ , and  $\partial_n U_x$  is the outward derivative normal to  $\Gamma_{back}$ . Here we used the chain-rule derivation  $\nabla \mathbb{1}_{\Omega_{back}}(\mathbf{x}) \cdot \mathbf{n} = -\left. \frac{dH}{du} \right|_{u=-U_x} \partial_n U_x(\mathbf{x})$ , and a higher-order generalisation of the one-dimensional relation

$$\int \phi(x) \frac{dH(x-x_0)}{dx} dx = \int \phi(x) \delta(x-x_0) dx = \phi(x_0), \tag{4.34}$$

namely:

$$-\iint_{\Omega} \phi(\mathbf{x}) \nabla \mathbb{1}_{\Omega_{back}}(\mathbf{x}) \cdot \mathbf{n} d\Omega = \iint_{\Omega} \phi(\mathbf{x}) \delta_{\Gamma_{back}}(\mathbf{x}) d\Omega = \oint_{\Gamma_{back}} \phi(\mathbf{x}) \tag{4.35}$$

where  $\delta_{\Gamma_{back}}$  is the two-dimensional delta function associated to  $\mathbb{1}_{\Omega_{back}}$ , and  $\mathbf{n}$  the outward normal of  $\Gamma_{back}$ . Therefore

$$\delta A_{back} = (\nabla_{\mathbf{U}} A_{back} | \delta \mathbf{U}) = -\oint_{\Gamma_{back}} \frac{\delta U_x}{\partial_n U_x} d\Gamma. \tag{4.36}$$

The sensitivity of  $A_{back}$  to volume control obtained using (4.36) is shown in figure 8. Regions of large sensitivity extend from upstream of the bump summit all the way to the reattachment point, with opposite signs below and above the separatrix.

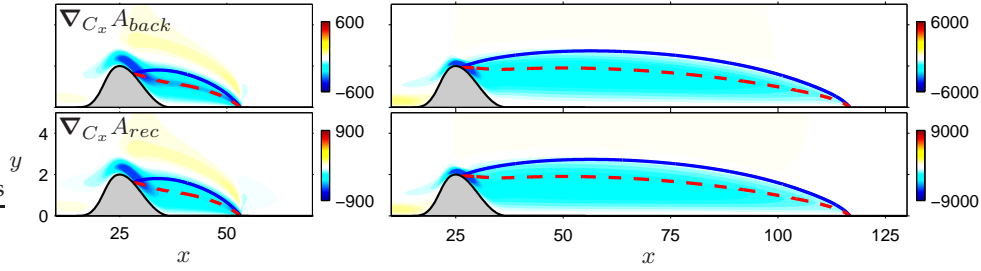


**Figure 8.** Sensitivity of backflow and recirculation areas  $A_{back}$ ,  $A_{rec}$ , with respect to streamwise volume control  $C_x$ . Left:  $Re = 100$ , right:  $Re = 500$ . The blue solid line is the separatrix, the red dashed line is the curve where  $U_x = 0$ .

### (d) Recirculation area

We first rewrite the recirculation area (2.4) as

$$A_{rec} = \iint_{\Omega} \mathbb{1}_{\Omega_{rec}}(\mathbf{x}) \, d\Omega = \int_{x_s}^{x_r} \int_{y_w(x)}^{y_{sep}(x)} dy \, dx \quad (4.37)$$

where we recall that  $y_w(x)$  describes the wall height and  $y_{sep}(x)$  the separatrix height. Then we notice that it is possible to give an Eulerian characterisation of the separatrix, namely that the flow rate through any vertical cross section of the recirculation region is zero:

$$\int_{x_s}^{x_r} \int_{y_w(x)}^{y_{sep}(x)} U_x(\mathbf{x}) \, dy \, dx = 0. \quad (4.38)$$

The sensitivity of the recirculation area with respect to flow modification is

$$\delta A_{rec} = \lim_{\epsilon \rightarrow 0} \frac{A_{rec}(\mathbf{U} + \epsilon \delta \mathbf{U}) - A_{rec}(\mathbf{U})}{\epsilon} \quad (4.39)$$

$$= \lim_{\epsilon \rightarrow 0} \frac{1}{\epsilon} \int_{x_s + \epsilon \delta x_s}^{x_r + \epsilon \delta x_r} \int_{y_w(x)}^{y_{sep}(x) + \epsilon \delta y_{sep}(x)} dy \, dx. \quad (4.40)$$

Next, we use (4.38) to obtain the first-order variation of the separatrix height:

$$\delta y_{sep}(x) = - \frac{1}{U_x(x, y_{sep}(x))} \int_{y_w(x)}^{y_{sep}(x)} \delta U_x(\mathbf{x}) \, dy. \quad (4.41)$$

Substituting into (4.40), splitting integration intervals into  $[y_w, y_{sep}] \cup [y_{sep}, y_{sep} + \epsilon \delta y_{sep}]$  and  $[x_s + \epsilon \delta x_s, x_s] \cup [x_s, x_r] \cup [x_r, x_r + \epsilon \delta x_r]$ , and keeping first-order terms finally leads to

$$\delta A_{rec} = (\nabla_{\mathbf{U}} A_{rec} | \delta \mathbf{U}) = \int_{x_s}^{x_r} \frac{-1}{U_x(x, y_{sep}(x))} \left( \int_{y_w(x)}^{y_{sep}(x)} \delta U_x(\mathbf{x}) \, dy \right) dx. \quad (4.42)$$

The sensitivity of  $A_{rec}$  to volume control obtained using (4.42) is shown in figure 8. As could have been expected, it is very similar to the sensitivity of the backflow area.

## 5. Results

### (a) Sensitivity maps

Figures 6, 7 and 8 already presented the sensitivity of all quantities of interest (2.1)-(2.4) to volume control. This sensitivity information can be used to compute the effect of a small control cylinder of diameter  $d$  inserted in the flow at  $(x_c, y_c)$ . This effect is modelled as a steady volume force

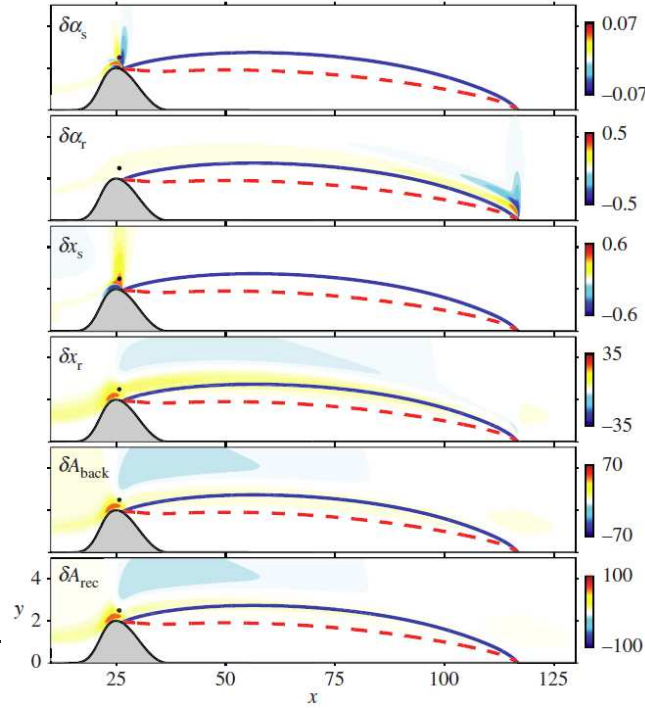


**Figure 9.** Effect of a control cylinder of diameter  $d = 0.05$  on separation and reattachment angles  $\alpha_s$ ,  $\alpha_r$ , stagnation points  $x_s$ ,  $x_r$ , backflow area  $A_{back}$  and recirculation area  $A_{rec}$ .  $Re = 500$ . The blue solid line is the separatrix, the red dashed line is the curve where  $U_x = 0$ . The black dot shows the position of the control cylinder  $(x_c, y_c) = (25.7, 2.5)$  used for validation in section 5(b).

opposed to the hypothetical drag force the control cylinder would feel if it were invested by the uniform flow  $\mathbf{U}(x_c, y_c)$ :

$$\delta \mathbf{C}(x, y) = -\frac{1}{2} d C_d(x, y) \|\mathbf{U}(x, y)\| \mathbf{U}(x, y) \delta(x - x_c, y - y_c) \quad (5.1)$$

where  $C_d$  is the cylinder drag coefficient. Its value depends on the local Reynolds number  $Re_d(x, y) = \|\mathbf{U}_b(x, y)\| d / \nu$ , which we compute from a fit of experimental and numerical data [15,19]. From (3.3) and (5.1), quantities of interest vary according to:

$$\delta \phi = (\nabla_{\mathbf{C}} \phi | \delta \mathbf{C}) = -\frac{1}{2} d C_d(\mathbf{x}_c) \|\mathbf{U}(\mathbf{x}_c)\| \nabla_{\mathbf{C}} \phi(\mathbf{x}_c) \cdot \mathbf{U}(\mathbf{x}_c). \quad (5.2)$$

Note that the predicted value  $\delta \phi$  varies linearly with the force, by construction, but non-linearly with the diameter of the control cylinder. Figure 9 shows the effect of a cylinder of diameter  $d = 0.05$  at  $Re = 500$ . The separation point and separation angle are mostly affected if the cylinder is inserted close to  $\mathbf{x}_s$ , and hardly vary otherwise. The reattachment angle is sensitive close to  $\mathbf{x}_r$ , and is weakly increased if the control cylinder is located in the shear layer. Overall, these three quantities appear robust since they cannot be modified easily (scales next to color bars confirm that their variations are of small amplitude). The reattachment point is much more sensitive and is predicted to move downstream if the control cylinder is inserted in the shear layer (particularly at the bump summit) or upstream, and should instead move slightly upstream for a cylinder farther away from the wall. Backflow and recirculation areas are affected in a fairly similar way, increasing when the control cylinder is located near the bump summit or upstream, and decreasing when the cylinder is farther above the bump or the early recirculation region.

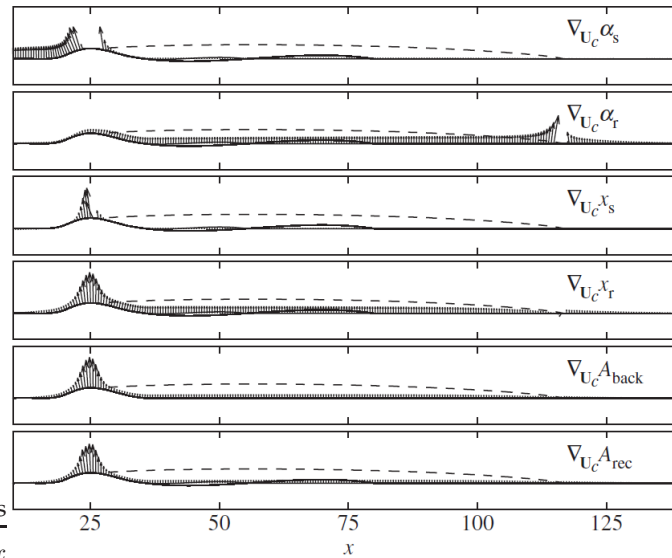


**Figure 10.** Sensitivity of separation and reattachment angles  $\alpha_s, \alpha_r$ , stagnation points  $x_s, x_r$ , backflow area  $A_{back}$  and recirculation area  $A_{rec}$  to wall control  $U_c$ . Arrows point in the direction of positive sensitivity. The dashed line is the separatrix.  $Re = 500$ .

Figure 10 shows sensitivity to wall control. Arrows point in the direction of positive sensitivity. All quantities are significantly more sensitive to normal actuation than to tangential actuation (axes are to scale, so that arrows show the actual orientation relative to the wall). Separation and reattachment angles are naturally most sensitive close to  $x_s$  and  $x_r$ , respectively. More interestingly,  $\alpha_s$  is also sensitive upstream of the bump and  $\alpha_r$  at the bump summit and in the whole recirculation region. The separation point  $x_s$  is sensitive only at the bump summit. Finally,  $x_r, A_{back}$  and  $A_{rec}$  are efficiently controlled by wall actuation at the bump summit and to a lesser extent in the whole recirculation region; unsurprisingly, these three quantities have very similar sensitivities. Note that the sensitivities of  $\alpha_s$  and  $x_s$  are very large at  $x_s$ , and the sensitivity of  $\alpha_r$  is very large at  $x_r$ ; for clarity, longest arrows at these locations are not shown.

Figures 9-10 allow to identify regions where quantities of interest are affected the most by control and to which extent.

## (b) Validation and control

In this section, we illustrate how control configurations can be designed based on sensitivity information. We also validate the method by comparing sensitivity predictions against non-linear results obtained from actually controlled flows at  $Re = 500$ .

Figure 11 shows how separatrix angles, stagnation locations, and backflow and recirculation areas vary when applying small-amplitude vertical wall suction ( $U_c = 0, V_c < 0$ ) over  $5 \leq x \leq 23$ , with total flow rate  $W$ . All quantities decrease, although not by the same amount: the reattachment point moves significantly upstream, inducing a large reduction in backflow and recirculation areas. Separatrix angles decrease only slightly. The separation point is virtually fixed, reminiscent of the fact that it is fairly independent of  $Re$  in the uncontrolled case (figure 4). The agreement between sensitivity predictions (straight solid lines) and actual results (symbols) is excellent at small flow rate. However, non-linear effects are non-negligible when  $|W| \gtrsim 0.1 - 0.2$  and in all cases, make actual variations smaller than predicted by sensitivity analysis.

Figure 12 shows variations of quantities of interest when a small control cylinder of diameter  $d = 0.05$  is inserted in the flow at  $\mathbf{x}_c = (x_c, y_c) = (25.7, 2.5)$  (this location is shown in figure 9 with

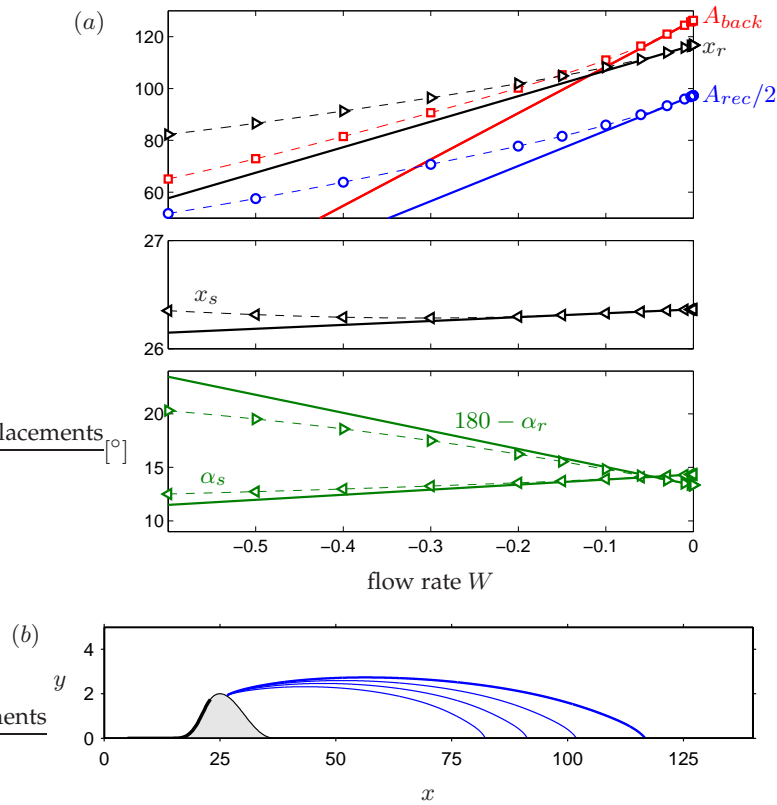


**Figure 11.** Effect of wall suction applied over  $5 \leq x \leq 23$  with total flow rate  $W$ , at  $Re = 500$ . (a) Variation of characteristic separation quantities (recirculation and backflow areas, stagnation locations, separation and reattachment angles). Thick solid lines show theoretical predictions from sensitivity analysis, while symbols show results from non-linear calculations. (b) Separatrix for the uncontrolled flow ( $W = 0$ , thick line), and  $W = -0.2, -0.4$  and  $-0.6$  (thin lines).

a black dot). All quantities increase with the cylinder diameter, especially the reattachment point and recirculation and backflow areas, while the separatrix angles and separation point are less affected. Again, non-linear effects are observed when  $d \gtrsim 0.05$ . This is consistent with the non-linear variations measured by Parezanović & Cadot [13] with  $d = 1$  mm and 3 mm. Recall that in addition to the non-linear effects neglected by our linear sensitivity analysis, variations (5.2) are linear in  $\delta C$  but not in  $d$  (since the drag coefficient depends on  $d$ ), therefore sensitivity predictions in figure 12 are not straight lines, unlike those in figure 11. We also report results obtained with the control cylinder included in the computational mesh (grey filled symbols) in order to assess the assumption of uniform flow underlying (5.1). Differences can be noticed when  $d \gtrsim 0.05$ , but sensitivity analysis does provide useful qualitative information regarding the influence of small passive control devices.

## 6. Conclusion

Considering the boundary layer flow above a wall-mounted bump as a prototype for separated flows, a variational technique was used to derive analytical expressions for the sensitivity of several geometric indicators of flow separation to steady actuation: the locations of the two stagnation points ( $x_s$  and  $x_r$ ), the angles of the separatrix ( $\alpha_s$  and  $\alpha_r$ ) at these points, the backflow area  $A_{back}$  and the recirculation area  $A_{rec}$ . For each geometric quantity, analytical expressions for the linear sensitivity to base flow modification  $\nabla_{U^*}$  were obtained. This gradient information

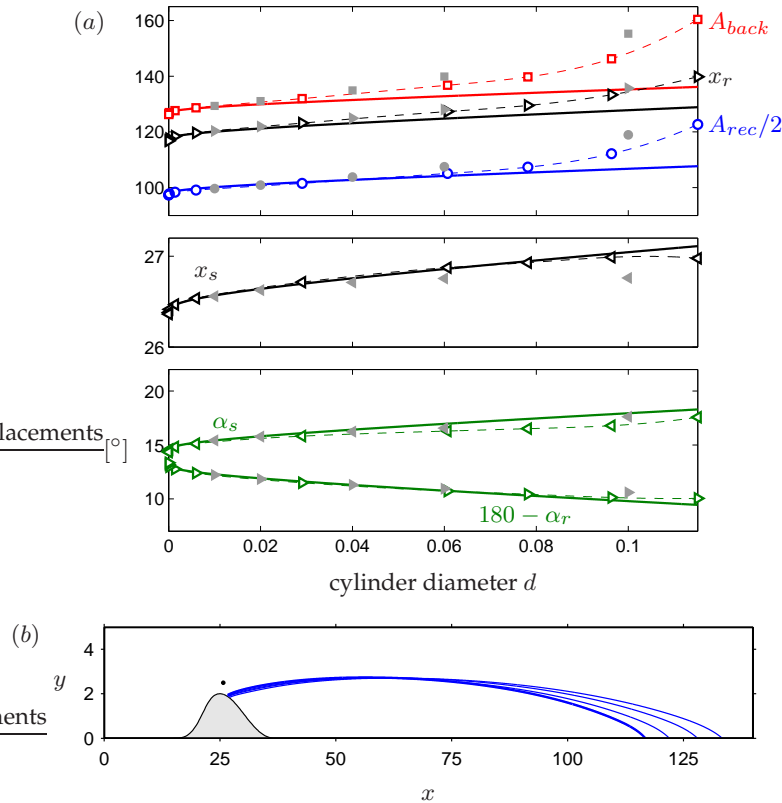


**Figure 12.** Effect of a small control cylinder of diameter  $d$  inserted in the flow at  $(x_c, y_c) = (25.7, 2.5)$ , at  $Re = 500$ . (a) Variation of characteristic separation quantities (recirculation and backflow areas, stagnation locations, separation and reattachment angles). Thick solid lines show theoretical predictions from sensitivity analysis while open symbols show results from non-linear calculations, both with the force model (5.1). Grey filled symbols show results from non-linear calculations with the control cylinder included in the mesh. (b) Separatrix for the uncontrolled flow (thick line) and for  $d = 0.02, 0.04$  and  $0.06$  (thin lines).

was further translated in sensitivity maps to localised volume forcing and wall blowing/suction through the introduction of the adjoint base flow, governed by linear adjoint equations forced by the previously determined gradient  $\nabla_{\mathbf{U}^*}$ . A suitable modelling of the addition of a small control cylinder as a localised force depending on the local velocity allowed to obtain sensitivity maps relevant to experimental studies.

Validations against full non-linear Navier–Stokes calculations showed an excellent agreement for small-amplitude control for all considered indicators. Non-linear effects appeared at larger amplitudes, consistent with experimental observations. With very resemblant sensitivity maps, the reattachment point, the backflow and recirculation areas were seen to be easily manipulated. In contrast, the upstream separation point and the separation and reattachment angles were found to remain extremely robust with respect to external steady actuation.

The present analysis, however, is limited to steady actuation and calls for a generalisation to the sensitivity of mean recirculation properties to harmonic forcing, which is known to be a more realistic, reliable and efficient experimental control scheme. Additionally, the recent development of fast imaging techniques has now made these geometric descriptors accessible in real-time [6], highlighting the need for the generalisation of current open-loop control optimisation tools to the dynamic closed-loop control of separation. The recent development of a solid theory for unsteady separation [3,29] provides a firm ground for this challenging objective.

## Acknowledgment

The authors thank Pierre-Yves Lagr e for an interesting discussion about Lighthill's original derivation of the separatrix angle, and for pointing to an Eulerian definition of the separatrix. This work was supported by the Swiss National Science Foundation (grant no. 200021-130315) and the French National Research Agency (project no. ANR-09-SYSC-001).

## References

- Seifert A, Pack Melton L.  
Identification and control of turbulent boundary layer separation, G ttingen, Germany, August 2004.  
In: Meier GEA, Sreenivasan KR, Heinemann HJ, editors. IUTAM Symposium on One Hundred Years of Boundary Layer Research. New York, NY: Springer; 2006. p. 199–208.
- Alam MR, Liu W, Haller G.  
Closed-loop separation control: An analytic approach.  
Physics of Fluids (1994-present). 2006;18(4).  
Available from: <http://dx.doi.org/10.1063/1.2188267>.
- Haller G.  
Exact theory of unsteady separation for two-dimensional flows.  
Journal of Fluid Mechanics. 2004 8;512:257–311.  
Available from: [http://journals.cambridge.org/article\\_S0022112004009929](http://journals.cambridge.org/article_S0022112004009929).
- Juillet F, Schmid PJ, Huerre P.  
Control of amplifier flows using subspace identification techniques.  
Journal of Fluid Mechanics. 2013 6;725:522–565.  
Available from: [http://journals.cambridge.org/article\\_S0022112013001948](http://journals.cambridge.org/article_S0022112013001948).
- Henning L, King R.  
Robust multivariable closed-loop control of a turbulent backward-facing step flow.  
Journal of Aircraft. 2007;44(1):201–208.  
Available from: <http://arc.aiaa.org/doi/abs/10.2514/1.22934>.
- Gautier N, Aider JL.  
Control of the separated flow downstream of a backward-facing step using visual feedback.  
Proceedings of the Royal Society A. 2013;469(2160).  
Available from: <http://dx.doi.org/10.1098/rspa.2013.0404>.
- Seifert A, Darabi A, Wagnanski I.  
Delay of airfoil stall by periodic excitation.  
Journal of Aircraft. 1996;33:691–698.  
Available from: <http://dx.doi.org/10.2514/3.47003>.
- Garnier E, Pamart PY, Dandois J, Sagaut P.  
Evaluation of the unsteady RANS capabilities for separated flows control.  
Computers & Fluids. 2012;61:39–45.  
Available from: <http://www.sciencedirect.com/science/article/pii/S0045793011002684>.
- McLachlan BG.  
Study of a circulation control airfoil with leading/trailing-edge blowing.  
Journal of Aircraft. 1989;26(2):817–821.  
Available from: <http://dx.doi.org/10.2514/3.45846>.
- Fiedler HE, Fernholz HH.  
On management and control of turbulent shear flows.  
Progress in Aerospace Sciences. 1990;27(4):305 – 387.  
Available from: <http://www.sciencedirect.com/science/article/pii/0376042190900022>.
- Wilson J, Schatzman D, Arad E, Seifert A, Shtende T.  
Suction and Pulsed-Blowing Flow Control Applied to an Axisymmetric Body.  
AIAA Journal. 2013;51(10):2432–2446.  
Available from: <http://dx.doi.org/doi:10.2514/1.J052333>.
- Pujals G, Depardon S, Cossu C.  
Drag reduction of a 3D bluff body using coherent streamwise streaks.  
Experiments in Fluids. 2010;49(5):1085–1094.  
Available from: <http://dx.doi.org/10.1007/s00348-010-0857-5>.

13. Parezanović V, Cadot O.  
Experimental sensitivity analysis of the global properties of a two-dimensional turbulent wake.  
*Journal of Fluid Mechanics*. 2012 2;693:115–149.  
Available from: [http://journals.cambridge.org/article\\_S0022112011004952](http://journals.cambridge.org/article_S0022112011004952).
14. Wang Y, Haller G, Banaszuk A, Tadmor G.  
Closed-loop Lagrangian separation control in a bluff body shear flow model.  
*Physics of Fluids (1994-present)*. 2003;15(8):2251–2266.  
Available from: <http://scitation.aip.org/content/aip/journal/pof2/15/8/10.1063/1.1588636>.
15. Boujo E, Gallaire F.  
Controlled reattachment in separated flows: a variational approach to recirculation length reduction.  
*Journal of Fluid Mechanics*. 2014 3;742:618–635.  
Available from: [http://journals.cambridge.org/article\\_S0022112014000238](http://journals.cambridge.org/article_S0022112014000238).
16. Zielinska BJA, Goujon-Durand S, Dušek J, Wesfreid JE.  
Strongly Nonlinear Effect in Unstable Wakes.  
*Phys Rev Lett*. 1997 Nov;79:3893–3896.  
Available from: <http://link.aps.org/doi/10.1103/PhysRevLett.79.3893>.
17. Choi H, Hinze M, Kunisch K.  
Instantaneous control of backward-facing step flows.  
*Applied Numerical Mathematics*. 1999;31(2):133 – 158.  
Available from: <http://www.sciencedirect.com/science/article/pii/S0168927498000317>.
18. Passaggia PY, Ehrenstein U.  
Adjoint based optimization and control of a separated boundary-layer flow.  
*Euro J Mech B/Fluids*. 2013;41:169–177.  
Available from: <http://dx.doi.org/doi:10.1016/j.euromechflu.2013.01.006>.
19. Boujo E, Ehrenstein U, Gallaire F.  
Open-loop control of noise amplification in a separated boundary layer flow.  
*Physics of Fluids*. 2013;25(12).  
Available from: <http://scitation.aip.org/content/aip/journal/pof2/25/12/10.1063/1.4846916>.
20. Taneda S.  
Experimental investigation of the wakes behind cylinders and plates at low Reynolds numbers.  
*Journal of the Physical Society of Japan*. 1956;11:302–307.  
Available from: <http://dx.doi.org/doi:10.1143/JPSJ.11.302>.
21. Acrivos A, Leal LG, Snowden DD, Pan F.  
Further experiments on steady separated flows past bluff objects.  
*Journal of Fluid Mechanics*. 1968;34:25–48.  
Available from: <http://dx.doi.org/10.1017/S0022112068001758>.
22. Nishioka M, Sato H.  
Mechanism of determination of the shedding frequency of vortices behind a cylinder at low Reynolds numbers.  
*Journal of Fluid Mechanics*. 1978 11;89:49–60.  
Available from: [http://journals.cambridge.org/article\\_S0022112078002451](http://journals.cambridge.org/article_S0022112078002451).
23. Barkley D, Gomes M Gabriela M, Henderson RD.  
Three-dimensional instability in flow over a backward-facing step.  
*Journal of Fluid Mechanics*. 2002;473:167–190.  
Available from: <http://dx.doi.org/10.1017/S002211200200232X>.
24. Marquillie M, Ehrenstein U.  
On the onset of nonlinear oscillations in a separating boundary-layer flow.  
*Journal of Fluid Mechanics*. 2003 8;490:169–188.  
Available from: [http://journals.cambridge.org/article\\_S0022112003005287](http://journals.cambridge.org/article_S0022112003005287).
25. Giannetti F, Luchini P.  
Structural sensitivity of the first instability of the cylinder wake.  
*Journal of Fluid Mechanics*. 2007;581:167–197.  
Available from: <http://dx.doi.org/10.1017/S0022112007005654>.
26. Passaggia PY, Leweke T, Ehrenstein U.  
Transverse instability and low-frequency flapping in incompressible separated boundary

- layer flows: an experimental study.  
Journal of Fluid Mechanics. 2012;703:363–373.  
Available from: <http://dx.doi.org/10.1017/jfm.2012.225>.
27. Ehrenstein U, Gallaire F.  
On two-dimensional temporal modes in spatially evolving open flows: The flat-plate boundary layer.  
J Fluid Mech. 2005;536:209–218.  
Available from: <http://dx.doi.org/doi:10.1017/S0022112005005112>.
28. Lighthill MJ.  
Introduction. Boundary layer theory.  
In: Rosenhead L, editor. Laminar Boundary Layers. Oxford University Press; 1963. p. 46–113.
29. Weldon M, Peacock T, Jacobs GB, Helu M, Haller G.  
Experimental and numerical investigation of the kinematic theory of unsteady separation.  
Journal of Fluid Mechanics. 2008 9;611:1–11.  
Available from: [http://journals.cambridge.org/article\\_S0022112008002395](http://journals.cambridge.org/article_S0022112008002395).